Vertical-Cavity Surface-Emitting Laser Active Regions for Enhanced Performance With Optical Pumping

Jon Geske, *Student Member, IEEE*, Kian-Giap Gan, Yae L. Okuno, Joachim Piprek, *Senior Member, IEEE*, and John E. Bowers, *Fellow, IEEE*

***Abstract*—We have developed an improved active region design for optically pumped vertical-cavity surface-emitting lasers. The design makes use of carrier-blocking layers to segment the absorber and promote uniform carrier populations in the quantum wells with pump efficiencies near 75%. A model to calculate the carrier distribution in the active region and a design methodology are presented along with a metric to describe the carrier uniformity in the quantum wells. Experimental verification of the performance improvements shows an over 50% reduction in device thresholds and an increase of 20 °C in maximum operating temperatures.**

***Index Terms*—Optical pumping, semiconductor lasers, surface-emitting lasers, wafer bonding.**

I. Introduction

VERTICAL-CAVITY surface-emitting lasers (VCSELs) are of great interest due to their advantages in low-cost manufacturing and packaging. In the pursuit of commercial-quality VCSELs operating at 1310 and 1550 nm, optically pumped VCSELs have been used not only as a development tools, but also in commercial products [1], [2]. In the design of optically pumped active regions it is desirable to make use of a long pump absorber region for high pumping efficiency. A long absorber is achieved by using the quantum-well barrier region as the absorber region. Carriers generated in the barrier diffuse to the quantum wells and provide gain for the lasing mode. Because no external bias is applied to an optically pumped device, there is little driving force to distribute the carriers among clusters of wells. Also, in VCSEL active regions it is advantageous for all quantum wells to be positioned as close as possible to the VCSEL cavity electric field standing wave peaks. For these reasons, research using optically pumped active regions with long absorbers has made use of active region designs with periodically spaced single quantum wells or clusters of quantum wells, each positioned on a standing wave peak of the longitudinal field the VCSEL oscillator [3], [4]. These periodic gain designs allow carriers optically generated in long barrier regions to diffuse directly to the nearest quantum-well region without passing over other clusters of wells.

Manuscript received March 17, 2004; revised June 8, 2004.

The authors are with the Electrical and Computer Engineering Department, University of California, Santa Barbara, CA 93106 USA (e-mail: geske@ece.ucsb.edu).

Digital Object Identifier 10.1109/JQE.2004.833234

Inherent in the periodic gain design is the exponential decay of the pump beam throughout the length of the barrier. Because of the exponential decay in the carrier generation rate, the quantum wells are not uniformly populated and the first quantum well is pumped harder than the last well. Material gain does not increase linearly with quantum-well carrier density so the first well produces less gain per carrier that the last well, resulting in a reduction in device efficiency and higher device thresholds and lower peak operating temperatures.

To improve the performance of optically pumped VCSELs and our recently demonstrated ultra-wideband wavelength division multiplexed VCSEL arrays [5], an improved optically pumped active region design has been developed and used for improved device performance [6]. We incorporate precisely placed carrier-blocking layers in the barrier to segment the absorber and control the diffusion of carriers to specific quantum-well regions. This improved segmented-absorber periodic gain (SAPG) active region design results in high pump efficiencies while simultaneously achieving uniform filling of the periodically spaced quantum-well regions. In Section II of this paper, a model for the carrier distribution in the traditional and new SAPG design is built. Section III then outlines a simplified design technique and presents traditional and SAPG active region designs for further numerical and experimental analysis. In Section IV, the proposed designs from Section III are analyzed using the model developed in Section II. The quantum-well injection uniformity C_{inj} is defined as a metric to compare the carrier uniformity in the quantum wells and is calculated for the new SAPG and traditional active region designs. In Section V, the results of this modeling and design work are then experimentally verified by building and comparing two optically pumped 1540-nm VCSEL structures utilizing each active region design. Section VI will discuss and compare the model and the experimental results.

II. Optically-Pumped VCSEL Active Region Model

Fig. 1 shows the conduction band diagram for a traditional optically pumped active region structure and for the new SAPG active region design concept. Both designs utilize a long barrier material designed to efficiently absorb the incident pump power. Fig. 1 illustrates the decay of a 980-nm pump beam incident upon each active region for a barrier material of 1.22-Q InGaAsP with an 18 000 cm^{-1} absorption coefficient. Between

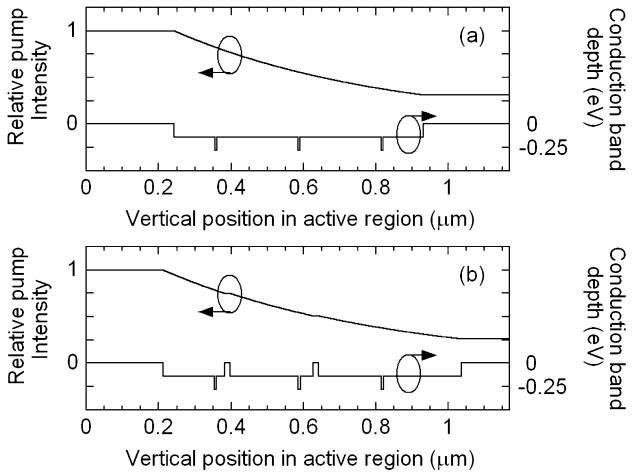

Fig. 1. Conduction band diagram and pump attenuation in traditional (a) segmented-absorber and (b) periodic gain optically pumped active region designs.

the wells of the new SAPG design are larger bandgap InP carrier-blocking layers. The purpose of these layers is to corral the optically generated carriers and force them to diffuse toward a specific quantum-well region. To determine the effect of these layers the carrier distribution in the barriers and the carrier density in each quantum well are desired. By determining the carrier density in each quantum well for different optical pumping conditions, the gain available from the traditional and new SAPG design can be compared and the laser threshold for both designs can be predicted. Knowledge of the carrier density in each quantum well allows for the calculation of the quantum-well injection uniformity, $C_{\rm inj}$, for each design.

We use the one-dimensional carrier diffusion equation to solve for the carrier distribution in both types of VCSEL active regions. To solve for the carrier distribution in all regions and all the quantum wells requires the numerical solution of a system of equations under steady-state conditions. We bound the problem by assuming there is no carrier flow over the InP layers in either active region design and by assuming the carrier density in the barrier is continuous across the thin quantum-well layer (or quantum-well region).

The steady-state carrier balance in the quantum well is given by

$$\frac{dn_{wi}}{dt} = \frac{n_{bi}}{\tau_c} - \frac{n_{wi}}{\tau_e} - \left(An_{wi} + Bn_{wi}^2 + Cn_{wi}^3\right) = 0. \quad (1)$$

The steady-state carrier balance in the continuous states above the quantum well is given by

$$\frac{dn_{bi}}{dt} = \frac{1}{t_{wi}}(J_{wi}^- - J_{wi}^+) - \frac{n_{bi}}{\tau_c} + \frac{n_{wi}}{\tau_e} = 0 \quad (2)$$

where n_{bi} is the carrier density in the continuous states above the ith quantum well, n_{wi} is the carrier density in the ith quantum well of t_{wi} thickness, τ_c is the capture time of carriers from the barrier into the quantum well, and τ_e is the thermal emission time of carriers out of the quantum well into the barrier. A, B, and C represent the defect, bimolecular, and auger recombination coefficients, and J_{wi}^+ and J_{wi}^- represent the carrier flux density into the continuous states above the quantum well from the left and right side. Multiple wells at each quantum-well region can be treated by modifying t_{wi} to be the cumulative thickness of all the quantum wells in the region.

In the barrier regions of the active region we are interested in the solution to the diffusion equation

$$D_a\frac{d^2n}{dx^2} - \frac{n}{\tau} + G = 0 \quad (3)$$

where the general form for the generation rate is given by

$$G' = G_0' e^{-\alpha x'}$$

and

$$G_0' = \frac{P_{\rm in}}{h\nu}\frac{\alpha}{\pi r^2}.$$

Here n is the carrier density in the barrier, D_a is the ambipolar diffusion coefficient in the barrier, τ is the ambipolar carrier lifetime in the barrier, α is the pump absorption coefficient, and $P_{\rm in}$ is the pump power incident on the active region at frequency ν and with a spot radius of r. The origin of the coordinate x' is located at the beginning of the active region barrier; hence it is shifted back from x by a length equal to the position of the barrier starting position. This must be accounted for in the final solution if this length is not zero (as is usually the case).

The general solution to (3) is given by

$$n(x) = C\sinh\left(\frac{x}{L_a}\right) + C'\cosh\left(\frac{x}{L_a}\right) + n_G e^{-\alpha x} \quad (4)$$

with the general form for n_G given by

$$n_G' = \frac{G_0'\tau}{1-(\alpha L_a)^2}$$

and the ambipolar diffusion length is

$$L_a = \sqrt{D_a\tau}.$$

To solve for the carrier distribution in the active region and the carrier densities in the quantum wells we build a system of equations in terms of the unknown values of J_{wi}^+ and J_{wi}^- and n_{bi} necessary to solve for n_{wi}, the carrier density in the quantum wells. The coupling of J_{wi}, n_{bi}, and n_{wi} in (1) and (2) requires a numerical solution for the final determination of the quantum-well carrier densities. For the traditional design all the regions are interdependent and are solved simultaneously. For the new SAPG design, each quantum-well region is separated from the other quantum-well regions by carrier-blocking layers. This separation allows each region to be solved independent of the other regions.

By applying the boundary conditions in the active regions, two types of solutions are attained. The first type is for a region bounded on one side by an InP barrier with no current flow over the barrier and bounded on the other side by a quantum well. This equation type is all that is needed to describe the new SAPG design with InP carrier-blocking layers between each well as shown in Fig. 1(b). The second type of equation is needed to fully describe the carrier distribution in the regions between the quantum wells of the traditional design of Fig. 1(a). This second type is bounded on both sides by quantum wells. In both solution types we rewrite the general solution in (4) by rewriting the constants C and C' in terms of the desired unknown variables

J_{wi}^{+} and J_{wi}^{-} and n_{bi} by using the relations $J_{wi} = -D_a(dn/dx)$ and $n = n_{bi}$ at the quantum-well position $x = X_i$.

We explore the development of the first equation type by looking at the first region to the left of the leftmost quantum well in Fig. 1(a). Here the InP blocking layer is at position $x = X_a$ and the quantum well is at position $x = X_1$. The boundary condition at the InP blocking layer is $dn/dx = 0$ because it is assumed that no current flows over the InP carrier-blocking layers. This boundary condition has been applied to yield

$$n_{b1}\sinh\left(\frac{W_0}{L_a}\right) + J_{wi}^{-}\frac{L_a}{D_a}\cosh\left(\frac{W_0}{L-a}\right) = n_G\left\{e^{-\alpha X_1}\left(\alpha L_a\cosh\left(\frac{W_0}{L_a}\right) + \sinh\left(\frac{W_0}{L_a}\right)\right) - \alpha L_a e^{-\alpha X_a}\right\}.$$

Here we have defined $W_0 = X_1 - X_a$ and

$$n_G = n_G' e^{\alpha X_a}.$$

The second equation type arises from applying the boundary conditions to the region located between the leftmost quantum well and center quantum well in Fig. 1(a). The quantum well on the left of this region is at position $x = X_1$ and the right well is at position $x = X_2$. The boundary conditions at the right well are $n = n_{b2}$ and $J_{w2} = -D_a(dn/dx)$ and have been applied to attain (5) and (6). We have defined $W_1 = X_2 - X_1$.

$$-n_{b1}\cosh\left(\frac{W_1}{L_a}\right) + n_{b2} + J_{w1}^{+}\frac{L_a}{D_a}\sinh\left(\frac{W_1}{L_a}\right) = n_G\left\{e^{-\alpha X_1}\left(\alpha L_a\sinh\left(\frac{W_1}{L_a}\right) - \cosh\left(\frac{W_1}{L_a}\right)\right) - e^{-\alpha X_2}\right\} \quad (5)$$

$$-n_{b1}\sinh\left(\frac{W_1}{L_a}\right) + J_{w1}^{+}\frac{L_a}{D_a}\cosh\left(\frac{W_1}{L_a}\right) - J_{w2}^{-}\frac{L_a}{D_a} = n_G\left\{e^{-\alpha X_1}\left(\alpha L_a\cosh\left(\frac{W_1}{L_a}\right) - \sinh\left(\frac{W_1}{L_a}\right)\right) - \alpha L_a e^{-\alpha X_2}\right\}. \quad (6)$$

Fig. 2 shows a schematic representation of the new SAPG VCSEL active region design. The total length of the active region is 5/2 lambda. Three quantum wells (or groups of quantum wells) are located on the middle three standing wave peaks in the cavity. A region on either side of the cavity, along the interface with the top and bottom distributed Bragg reflector (DBR), is reserved for superlattice structures that are used in the final wafer-bonded VCSEL for wavelength control and growth rate error adjustment [7]. The barrier material is designed to absorb the pump beam while the InP carrier-blocking layers, located on either side of each quantum well, are transparent at the pump wavelength. The position of the carrier-blocking layers can be adjusted anywhere in the range between the quantum wells or between a quantum well and the area reserved for the superlattice regions. Minimum setback distances are used between the center of the carrier-blocking layer and the center of the quantum wells and between the edge of the carrier-blocking layers and the superlattice region on each side of the active region.

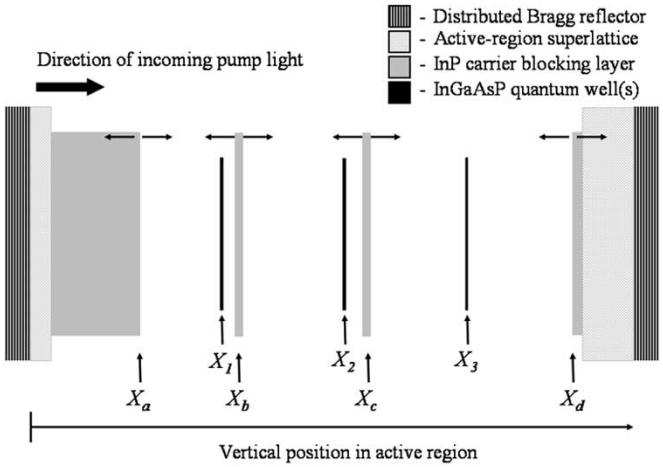

Fig. 2. Schematic representation of the new SAPG VCSEL active region design.

Similar equations can be built by applying similar boundary conditions for the other regions of the optically pumped active region designs shown in Fig. 1. Using these equations, along with (2) and (1) for each quantum well, a system of equations can be built and solved numerically for each quantum well (or cluster of wells). From this solution, the unknown quantities J_{wi}^{+} and J_{wi}^{-}, n_{bi}, and the quantum-well carrier density n_{wi} can be determined. Together the quantities J_{wi}^{+} and J_{wi}^{-}, n_{bi} determine the coefficients C and C' of (4) which describe the complete carrier distribution in the barrier regions.

Once the carrier density in each quantum well is know for each design, the available material gain from each well is determined via a numerical free-carrier gain model including bandgap renormalization, as implemented in PICS3D by Crosslight Software, Inc. We can then directly compare the effect the new carrier-blocking layers have on the overall performance of the active region. Prior to completing the model however, the specific structure of the active region design must be specified. This is accomplished by a design optimization approach.

III. Optically Pumped VCSEL Active Region Design

By using carrier-blocking layers positioned between quantum-well regions, it is possible to compensate for the exponential decay of the carrier generation rate along the vertical length of the active region. In order to attain uniform carrier density in each quantum well of the periodic gain structure, it is necessary to position the carrier-blocking layers in a manner that allows an equal number of carriers to diffuse into each well. To accomplish this goal, an iterative optimization approach has been utilized in the design of the active region. This approach allows for the simultaneous maximization of the amount of pump power absorbed while maintaining uniform carrier densities in each well. This approach has been generalized to allow for multiple quantum wells at each standing wave peak in the periodic gain structure.

The design objective is to maximize the total absorber length while achieving an equal number of optically generated carriers in each region. Accounting for the transparent carrier-blocking layers of thickness t_b located between each well, the pump power in the absorbing barrier regions along the horizontal axis of the active region in Fig. 2 is given by

$$P(x) = \begin{cases} P_{\text{in}} e^{-\alpha(x - X_a)} & X_a \le x \le X_b - \dfrac{t_b}{2} \\ P_{\text{in}} e^{-\alpha(x - X_a - t_b)} & X_b + \dfrac{t_b}{2} \le x \le X_c \dfrac{t_b}{2} \\ P_{\text{in}} e^{-\alpha(x - X_a - 2t_b)} & X_c + \dfrac{t_b}{2} \le x \le X_d \end{cases}.$$

Here we have neglected any pump power reflection at the interfaces. Given this pump power distribution, in order for each barrier region to have an equal number of optically generated carriers the following condition must be true:

$$\frac{1}{m_1} \int_0^{X_b - X_a - t_b/2} e^{-\alpha u}\, du = \frac{1}{m_2} \int_{X_b - X_a - t_b/2}^{X_c - X_a - 3t_b/2} e^{-\alpha u}\, du = \frac{1}{m_3} \int_{X_c - X_a - 3t_b/2}^{X_d - X_a - 2t_b} e^{-\alpha u}\, du \quad (7)$$

where m_1, m_2, and m_3 are the number of quantum wells at each position. From this relation we find

$$X_c = -\frac{1}{\alpha} \ln \left[\left(1 + \frac{m_2}{m_1}\right) e^{-\alpha(X_b - X_a - t_b/2)} - \frac{m_2}{m_1} \right] + X_a + \frac{3t_b}{2}$$

$$X_d = -\frac{1}{\alpha} \ln \left[\left(1 + \frac{m_3}{m_2}\right) e^{-\alpha(X_c - X_a - 3t_b/2)} - \frac{m_3}{m_2} e^{-\alpha(X_b - X_a - t_b/2)} \right] + X_a + 2t_b.$$

Thus, by selecting the appropriate X_a and X_b, we can find the ideal solution that allows for the greatest pump power absorption while equalizing the number of carriers generated in each region for each quantum well. In practice this is done by an iterative maximization of the difference between X_d and X_a while satisfying (7) and not violating any of the defined carrier-blocking layer setback requirements. The actual problem is solved in relative units in terms of fractional wavelengths inside the material.

For our optically pumped VCSEL design we use a 980-nm laser as the optical pump source and we have chosen the photoluminescence peak of our quantum wells to be at 1520 nm. The barrier and pump absorber used is 1.22-Q InGaAsP because it has a high absorption coefficient measured to be 18 000 cm^{-1} at 980 nm and provides a conduction band depth of 80 meV for electron confinement. In addition, the group III composition used in the 1.22-Q barrier is identical to that used in the quantum wells, facilitating the growth of high quality wells. Our active region is designed for use in a wavelength division multiplexing (WDM) array and hence has several superlattice periods on each side. This places a front side (left side in Fig. 2) setback of 40 nm and a backside setback of 135 nm. Single quantum wells are used at each standing-wave peak, hence $m_1 = m_2 = m_3 = 1$. The average index of the barrier material is calculated to be 3.35 at the lasing wavelength of 1540 nm and the quantum wells are positioned at wavelength units of 0.75, 1.25, and 1.75. The minimum gap allowed between the center of the two central 15-nm thick carrier-blocking layers and the center of the 5-nm thick quantum wells is 25 nm.

TABLE I
NEW SAPG ACTIVE REGION DESIGN EPITAXIAL LAYER BOUNDARY POSITIONS

Total active region length	1171.6 nm
Xa	212.1 nm
Xb	382.1 nm
Xc	627.7 nm
Xd	1036.6 nm
X1	357.1 nm
X2	588.7 nm
X3	818.6 nm

TABLE II
TRADITIONAL ABSORBER DESIGN EPITAXIAL LAYER BOUNDARY POSITIONS

Total active region length	1174.7 nm
Front Cladding	243.0 nm
Well 1	357.8 nm
Well 2	587.4 nm
Well 3	817.0 nm
Back Cladding	931.7 nm

Based on our design parameter requirements and the design optimization approach presented here, we have calculated the new SAPG active region parameters shown in Table I. This design gives a total expected absorption of about 74%.

For comparison purposes, Table II shows a traditional periodic gain structure with symmetric absorbers. This design gives a total expected absorption of about 69%.

IV. VCSEL ACTIVE REGION MODELING RESULTS

The specific traditional and new SAPG active region designs shown in Tables I and II can be directly compared using the carrier diffusion model developed. Additional parameters used in the model are shown in Table III. $R_{\text{top}}, R_{\text{bottom}}, \Gamma_{\text{enh}}, L_m$, and g_{th} are calculated using well known techniques.

The recombination coefficient A and the internal loss α_i are used as fit parameters in the final model calculations to match the measured threshold of the VCSEL device fabricated using the new SAPG active region. The recombination parameter used includes carrier loss due to radial carrier diffusion and defect recombination and results in a larger than expected recombination parameter [11]. The internal loss value chosen is consistent with values typically used in VCSELs.

Using the parameters in Table III and the specific active-region geometries given in Section III the carrier distribution in both active region designs has been calculated by applying the model developed in Section II. Figs. 3 and 4 show the results of these calculations. For comparison purposes, data is shown at the pump power input level necessary for equal total absorbed power in both designs. The absorbed pump power level used corresponds to 0.5 mW, the level necessary to reach threshold in the VCSEL based on the new SAPG active region design. Based

TABLE III
PARAMETERS USED IN MODEL CALCULATIONS

T	Temperature	293 K
τ	Ambipolar carrier lifetime in barriers	7.9 ns [8]
D_a	Ambipolar diffusion coefficient	7.4 cm^2/sec [8]
τ_c	Net quantum well capture time	0.25 ps [9]
A	Defect recombination (fit parameter)	3 ns^{-1}
B	Bimolecular recombination	$0.3x10^{-10}$ cm^3/sec [10]
C	Auger recombination	$6x10^{-29}$ cm^6/sec [10]
r	980-nm pump radius	2.5 μm
α_i	VCSEL internal loss (fit parameter)	10 cm^{-1}
R_{top}, R_{bottom}	VCSEL mirror reflectivity (GaAs/AlAs)	0.99914, 0.999966
Γ_{enh}	Traditional design gain enhancement factor	1.95381
Γ_{enh}	New design gain enhancement factor	1.92539
L_m	Mirror penetration depth	0.755 μm
g_{th}	Traditional design average threshold material gain	1069 cm^{-1}
g_{th}	New design average threshold material gain	1083 cm^{-1}

on the expected absorption efficiencies of the two different designs, 0.5 mW of absorbed power corresponds to an input pump power of 0.68 mW for the new SAPG active region design and 0.76 mW for the traditional active region design.

The model calculations predict more uniform carrier filling of the wells in the new design as is evident from a comparison of Figs. 3 and 4. This uniformity translates into more uniform gain from each well of the new design as shown in Fig. 5. The figure also shows all quantum wells of the traditional design have not yet reached transparency. Due to gain saturation effects and limitations on the highest carrier density that can be achieved in a quantum well, this carrier nonuniformity will results in higher device thresholds and less efficient device operation. The model predicts a modest 4.9% improvement in threshold with the new design.

Based on the carrier density in each quantum well, it is possible to quantify the quantum-well injection uniformity, C_{inj}, in each device. We define C_{inj} as the ratio of the standard deviation to the mean of the carrier density in the quantum wells, $C_{\mathrm{inj}} = \sigma/\mu$. It is desirable to minimize C_{inj} in an active region design to most efficiently generate gain from the available carriers. C_{inj} is 0.0113 and 0.212 in the new SAPG and the traditional designs respectively.

V. EXPERIMENTAL RESULTS

In order to validate the design and the model, two optically pumped VCSEL structures were fabricated. Both active-regions used the layer designs of Section III with three 5-nm wide 1% compressively strained InGaAsP quantum wells. The photoluminescence peaks were identical in both wafers and were

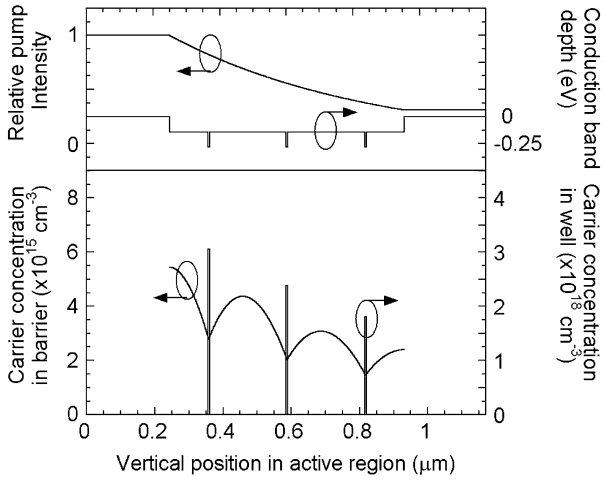

Fig. 3. Predicted carrier distribution in barrier and quantum-well carrier density in traditional optically pumped active region design.

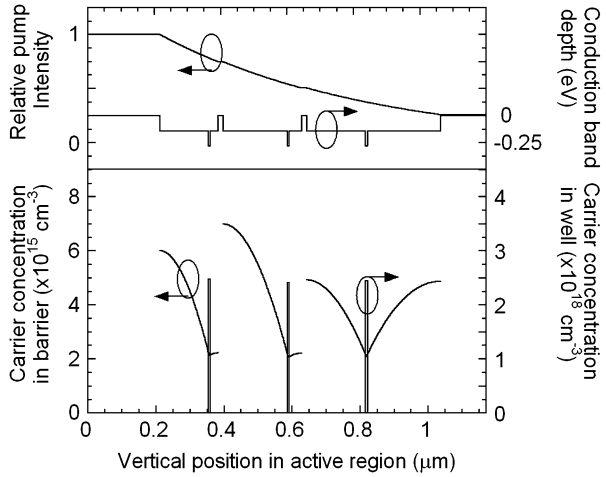

Fig. 4. Predicted carrier distribution in barrier and quantum-well carrier density in new SAPG optically pumped active region design.

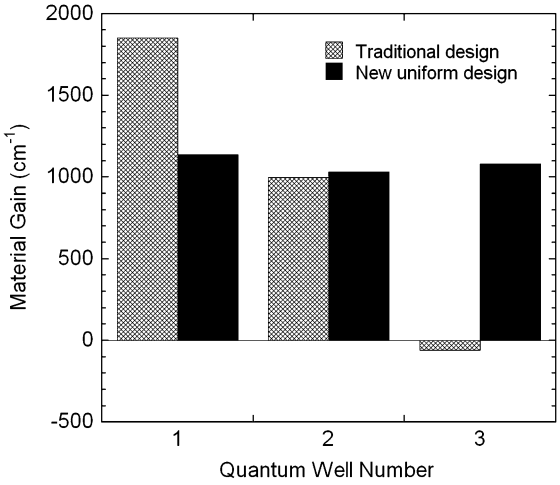

Fig. 5. Predicted quantum-well gain in traditional and new SAPG active region designs. Data shown is calculated at the new design's threshold absorbed pump power of 0.5 mW.

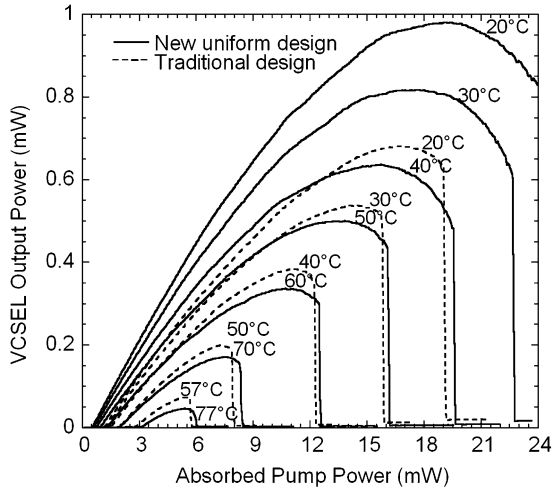

Fig. 6. Light-out versus absorbed light-in over temperature for VCSEL structures using both traditional and new SAPG active region designs.

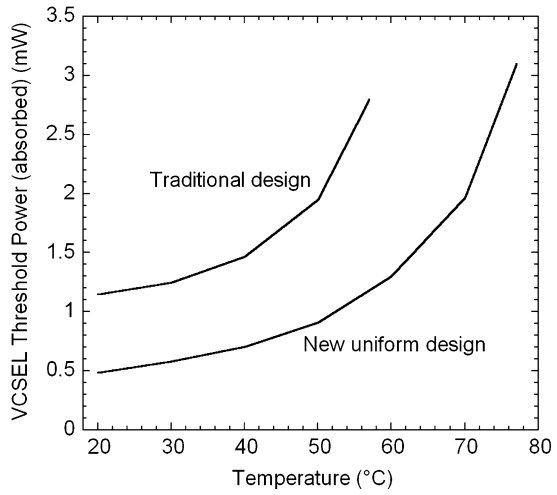

Fig. 7. Measured VCSEL thresholds over temperature for VCSEL structures using both traditional and new SAPG active region designs.

located at 1520 nm. The optically pumped VCSEL devices were fabricated by wafer bonding [12] a 40-period GaAs/AlAs bottom DBR and a 24.5-period GaAs/AlAs top DBR. The top mirror reflectivity included an in-phase semiconductor-air interface reflection. The device was optically pumped from the bottom with 980-nm laser emission focused to a 5-μm spot. The completed VCSELs emitted single-mode at 1540 nm. Light-out vs. light-in results over temperature are shown in Fig. 6. For the purposes of accurate comparison, the approximate amount of power actually absorbed in each active region design has been estimated from measurements and is plotted along the abscissa of Fig. 6. Multiple devices were tested from two process runs and the data shown here is from devices representative of the both sets of samples.

The absorption efficiencies of the tested VCSELs based on the new and traditional active region designs were calculated to be 84% and 78%. These values are calculated based on measurements made of the pump incident on the sample and passing through the sample and by accounting for the air-semiconductor reflections on the top and bottom of the sample. Measurements made on similarly prepared samples with no VCSEL epitaxial structures have shown a 10% scattering loss of the back of the manually polished substrate upon which the pump beam is incident. By neglecting this backside scattering loss and all interface reflections inside the VCSEL, the 84% and 78% pump efficiency values calculated from the tested devices overestimate the actual values which are likely closer to the ideal expected values of 74% and 69%.

Fig. 7 shows the threshold variation with temperature for both VCSEL designs. The SAPG design has a room temperature threshold of 0.49 mW while the traditional design has a 1.2 mW threshold. This represents a threshold improvement of over 50% with the new design. Fig. 8 shows the peak output power over temperature for both designs. The SAPG design shows a 20 °C improvement in peak operating temperature and continues to operate up to 77 °C. The enhanced output power of the SAPG design is coupled to the improved operating

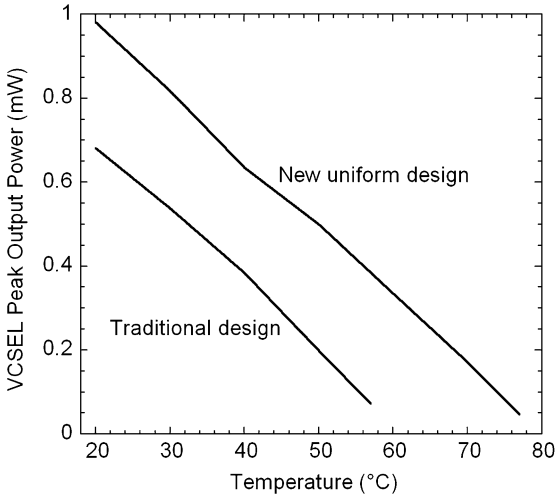

Fig. 8. Measured VCSEL peak output power over temperature for VCSEL structures using both traditional and new SAPG active region designs.

temperature of the new design. This improved temperature performance allows the VCSEL with the new SAPG active region to operate at higher pump powers and thus reach higher output powers. Both designs have the same thermal impedance of 0.89 °C/mW and nearly identical operating wavelengths and PL wavelengths. Because great care was taken to ensure all other parameters were equal, these VCSEL improvements are attributed to the improved carrier uniformity achieved with the new SAPG active region design.

VI. Summary and Discussion

An active region designed specifically for efficient optical pumping has been presented. The design makes use of a long pump absorber region for efficient pump absorption, and precisely placed carrier-blocking layers for uniform carrier filling of the quantum wells. A model to describe the carrier distribution in the active region and a design method has been developed and presented. The new design approach has been applied to a 5/2-wavelengths thick periodic gain VCSEL active region with

one quantum well on each of the three central standing wave peaks of the cavity. The model shows that pump efficiencies of 74% can be achieved while simultaneously filling each of the three quantum wells with a uniform number of carriers. The quantum-well injection uniformity parameter C_{inj} has been introduced as the ratio of the standard deviation to the mean value of the carrier density in the different quantum wells of the active region. This parameter has been calculated for the new and traditional designs and found to be 0.0113 and 0.212, respectively. Experimental results verify that the new design improves the threshold by over 50% and the peak operating temperature by 20 °C.

The results of the model and the experiment shown the same trend toward improved thresholds with the new design, but do not agree well quantitatively. The use of the defect recombination parameter and the VCSEL internal loss as fitting parameters in the model was not sufficient to simultaneously match the model to the experimentally measured threshold values for the VCSELs with the traditional and SAPG active region designs. This mismatch is due to a combination of the simplistic nature of the diffusion model used, and the lack of precision in the gain model. Because the improved uniformity of the carrier population in each well the new design avoids the gain saturation effects that can occur in quantum wells, errors in the differential gain of the gain model will translate into changes in the predicted improvement with the new design. It is postulated that the gain model used overestimates the amount of gain generated in the first well shown in Fig. 5. Regardless of their quantitative differences, both the experiment and the model demonstrate the improved performance of the new SAPG active region design. The use of a segmented-absorber in optically pumped VCSELs with periodic gain active regions can lead to improved temperature, threshold, and output power performance.

REFERENCES

[1] V. Jayaraman, T. Goodnough, T. Beam, F. Ahedo, and R. Maurice, "Continuous-wave operation of single-transverse-mode 1310-nm VCSELs up to 115 degrees C," *IEEE Photon. Technol. Lett.*, vol. 12, pp. 1595–1597, Dec. 2000.

[2] D. Vakhashoori, P. D. Wang, M. Azimi, K. J. Knopp, and M. Jiang, "MEMs-tunable vertical-cavity surface-emitting lasers," presented at the Optical Fiber Communication Conference and Exhibit, Paper TuJ1, Anaheim, CA, Mar. 17–22, 2001.

[3] C. Symonds, L. Sagnes, J.-L. Oudar, S. Bouchoule, A. Garnache, J. Baggren, and M. Strassner, "Room temperature CW operation at 1.55 μm of a monolithic InP-based optically pumped vertical-external-cavity surface-emitting lasers grown by MOCVD," in *Proc. 2003 Int. Conf. Indium Phosphide and Related Materials* Piscataway, NJ, 2003, pp. 259–260.

[4] J. Hastie, J.-M. Hopkins, S. Calvez, C. Jeon, D. Burns, R. Abram, E. Riis, A. Ferguson, and M. D. Dawson, "0.5-W single transverse-mode operation of an 850-nm diode-pumped surface-emitting semiconductor laser," *IEEE Photon. Technol. Lett.*, vol. 15, pp. 894–896, July 2003.

[5] J. Geske, D. Leonard, M. MacDougal, Y. L. Okuno, J. Piprek, and J. E. Bowers, "Long-wavelength WDM vertical-cavity surface-emitting laser arrays spanning 140 nm," presented at the European Conf. Optical Communications, Paper We4.P.79, Rimini, Italy, Sept. 21–25, 2003.

[6] J. Geske, D. Leonard, M. H. MacDougal, B. Barnes, and J. E. Bowers, "CWDM vertical-cavity surface-emitting laser array spanning 140 nm of the C, S, and L fiber transmission band," *IEEE Photon. Technol. Lett.*, vol. 16, pp. 1227–1229, May 2004.

[7] J. Geske, Y. L. Okuno, D. Leonard, and J. E. Bowers, "Long-wavelength two-dimensional WDM vertical cavity surface-emitting laser arrays fabricated by nonplanar wafer bonding," *IEEE Photon. Technol. Lett.*, vol. 15, pp. 179–181, Feb. 2003.

[8] S. Juodkazis, M. Petrauskas, A. Quacha, and M. Willander, "Charge carrier recombination and diffusion in InGaAs(P) epitaxial layers," *Physica Status Solidi A*, vol. 140, no. 2, pp. 439–443, Dec. 1993.

[9] H. Hirayama, J. Yoshida, Y. Miyake, and M. Asada, "Estimation of carrier capture time of quantum-well lasers by spontaneous emission spectra," *Appl. Phys. Lett.*, vol. 61, no. 20, pp. 2398–2400, Nov. 1992.

[10] L. A. Coldren and S. W. Corzine, *Diode Lasers and Photonic Integrated Circuits*. New York: Wiley , 1995, p. 170, 159.

[11] S. Bjorlin, "Long-wavelength vertical-cavity semiconductor optical amplifiers," Ph.D. Dissertation, Dept. Elect. and Comp. Eng., Univ. California, Santa Barbara, CA, 2002.

[12] A. Black, A. R. Hawkins, N. M. Margalit, D. I. Babic, A. L. Holmes Jr., Y. Chang, P. Abraham, J. E. Bowers, and E. L. Hu, "Wafer fusion: Material issues and device results,"," *IEEE J. Select. Topics Quantum Electron.*, vol. 3, pp. 943–951, June 1997.

Jon Geske (S'97) received the B.S. degree in electrical engineering from the University of Southern California in 1997 and the M.S. degree in 2001 from the University of California, Santa Barbara (UCSB).

Prior to attending UCSB, he worked for two years at Gore Photonics where he developed novel fabrication techniques for long-wavelength vertical-cavity surface-emitting lasers (VCSELs). His current research area at UCSB is in the development of advanced heterogeneous integration techniques for two-dimensional wavelength division multiplexing VCSEL arrays.

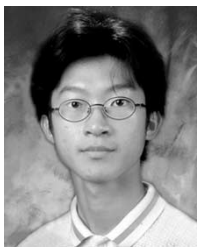

Kian-Giap Gan was born in Johor, Malaysia, in 1976. He received the B.S. degree in electrical engineering from National Taiwan University, Taipei, Taiwan, in 1999. He is currently working toward the Ph.D. degree in electrical engineering at the University of California, Santa Barbara.

His current research interests include the study of high-speed optoelectronics devices and materials.

Yae L. Okuno received the B.S. degree in nuclear engineering from Kyoto University, Kyoto, Japan in 1990, and the M.S. degree in electrical engineering from the University of California, Berkeley, in 1999.

From 1990 to 1997 she was with the Hitachi Central Research Laboratory, Tokyo, Japan, where she worked on MOVPE of InP and GaAs, long-wavelength lasers, and wafer-fusion. She joined the University of Southern California, Santa Barbara, in 1999. Her research interests are wafer-fused vertical-cavity surface-emitting lasers and MOVPE of InP and related materials.

Joachim Piprek (M'94–SM'98) received the Ph.D. degree in solid-state physics from Humboldt University, Berlin, Germany, in 1986.

He is currently an Adjunct Associate Professor at the University of Southern California, Santa Barbara. He has worked in industry and academia on design and analysis of optoelectronic devices and has given more than 40 invited talks, seminars, and short courses in this field. He has authored more than 50 papers in refereed journals, two book chapters, and a book entitled *Semiconductor Optoelectronic Devices—Introduction to Physics and Simulation* (New York: Academic, 2003).

Dr. Piprek chairs the SPIE Symposium on Semiconductor Optoelectronic Devices for Lightwave Communication as well as the annual International Conference on Numerical Simulation of Semiconductor Optoelectronic Devices.

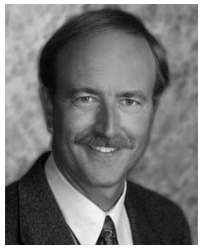

John E. Bowers (S'78–M'81–SM'85–F'93) received the M.S. and Ph.D. degrees from Stanford University, Stanford, CA.

He is the Director of the Multidisciplinary Optical Switching Technology Center (MOST), and a Professor in the Department of Electrical Engineering at the University of California, Santa Barbara (UCSB). He previously worked for AT&T Bell Laboratories and Honeywell before joining UCSB. He is cofounder of the Center for Entrepreneurship and Engineering Management, a founder of Terabit Technology and Calient Networks, and serves on the Board of Directors of Calient Networks. He has published 6 book chapters, over 350 journal papers, over 506 conference papers, and has received 32 patents. His research interests are primarily concerned with optoelectronic devices and optical networking.

Dr. Bowers is a Fellow of the Optical Society of America and the American Physical Society, and a recipient of the IEEE Lasers and Electro-Optics Society (LEOS) William Streifer Award.